Execution Time Reduction and Weighting Factor Elimination in FCS-MPC for High-level Converters

Aria Veysinejad
Department of Electrical Engineering
K.N. Toosi University of Technology
Tehran, Iran
aria.vn@email.kntu.ac.ir

Saman Rahmati
Department of Electrical Engineering
K.N. Toosi University of Technology
Tehran, Iran
rahmati@email.kntu.ac.ir

Mohammad Tavakoli Bina
Department of Electrical Engineering
K.N. Toosi University of Technology
Tehran, Iran
tavakoli@eetd.kntu.ac.ir

***Abstract*— The Finite set model predictive control method (FCS-MPC) is a well-known controller. FCS-MPC is a multi-objective control method with a fast transient response which can be utilized widely in various applications. However, this control method suffers from high computational burden besides its numerous benefits. Also, tuning weighting factors are required to deal with different control objectives which, is another drawback of this controller. This paper proposes a targeted search procedure to suppress high computational burden and eliminate weighting factors in the FCS-MPC. A nine-level converter that connects photovoltaic modules to the gird is considered as an example to explain the proposed procedure. In this regard, the conventional FCS-MPC method divided into three steps which, each step targets one control objective with much lower execution time. Hence, along with the significant computational burden reduction, the weighting factors are eliminated too. The simulations are carried out in MATLAB-Simulink environment and results compared with the conventional method in the steady-state and transient conditions to illustrate the performance of the proposed method.**

Keywords*— *FCS-MPC, High-level converter, computational time reduction, weighting factor elimination

I. INTRODUCTION

Multilevel inverters aim to suppress the two-level inverter limitation. Compared to the two-level inverter, multilevel inverters offer several improvements, such as high voltage ability, high power quality, low switching losses, low dv/dt, low current and voltage harmonics, smaller filter, capability of distributing voltage stress among devices, etc. [1]. Four topologies of flying capacitor (FC), neutral point clamped (NPC), cascaded H-bridge (CHB) and modular multilevel converter (MMC) are the most known MIs [1-3]. In NPC inverter as voltage level increases the number of clamping diodes increases significantly. At high number of voltage levels, the revers recovery times of diodes encounter the appliance of this topology with obstacles [4]. The major disadvantage of FC is high number of capacitors and, as for NPC, it is not suitable for high number of voltage levels [4]. MMC topology can eliminate the FC and NPC shortcomings. MMC, the same as FC and NPC, needs a common dc link. However, in some applications that provide individual DC voltages, such as photovoltaic (PV) farms, another topology is more attractive. For example, to achieve high voltage dc link in a PV farm, large number of PV modules can be connected in series that will affect the maximum power point tracking (MPPT) operation of PV modules. Moreover, series connected PV modules will increase losses, because of their series connected resistors. To overcome the mentioned drawbacks, DC voltage regulators, such as boost converter, can use in each PV module, as [5]. However, it will increase the total cost and semiconductor losses. Another topology that can be used in high voltage and high-level application is CHB inverter. CHB can also eliminate the large number of series connected PV modules and DC voltage regulator. Cascaded inverter can provide one converter per PV panel [6].

In order to control the MI topologies, pulse width modulation (PWM) and space vector modulation (SVM) are the most known methods [7]. Due to advances in microprocessor technologies with high computational power, using more complex control methods seem to become practically feasible, such as fuzzy and predictive control. Finite-control-set model predictive control (FCS-MPC) is another control method, which is more recently appeared as an attractive and powerful control method [8,9]. FCS-MPC is a multi-objective control method which is satisfactory when dealing with numerous control parameters is needed, e.g., current tracking, capacitor voltage balancing, switching frequency and losses reduction [10-12]. The high computational burden is the main drawback of FCS-MPC which, affects the overall performance of the controller. The computational burden increases as the complexity of the converter or the number of control objectives increases.

This matter has taken into account for different applications in some literature [13-15]. Paper [13] divides computational burden of FCS-MPC between a group of microcontrollers to decrease the calculation time. However, this method has no effect on computational burden and just decreases computational time. Papers [13,14] narrow the searched states by considering different situations and sectioning the state space vector area. [16] used the simple Euler forward method to reduce the computational effort and [17] proposed two-stage model predictive control method for a 3-level NPC. At first step in [17], the largest voltage vectors have been considered and at the second step only the nearest small and medium voltage vectors to the optimal large vector have been investigated. In order to decrease the number of predicted states of FCS-MPC, preselection algorithm has proposed for MMC in [18] and, [19] has used graph algorithm method for CHB. However, the proposed algorithm in [18] is complicated and, reference [19] did not consider the voltage balancing and just observed the output current in the cost function.

In this paper, a three-phase structure of nine-level CHB-NPC is used to connect the individual DC voltages to the three-phase grid where, PV modules are considered as individual DC voltages. Single-phase model of this topology, which is proposed in [8], has 81 switching states and it will increase to 81^3 in three-phase structure. This paper aims to reduce the computational burden magnificently regarding FCS-MPC control of this topology, while achieving MPPT

operation in PV modules and capacitor voltage balancing at the DC side and attain smooth and low harmonic current at the AC side. In this regard, the utilized inverter topology introduced at II. In section III, FCS-MPC and the used cost function is presented. The proposed method to decrease the computational burden has been discussed in the further section (IV). After all, simulation results and conclusion is presented in sections V and VI respectively.

II. General Description

A. Plant Model

To connect the individual DC-Links to the grid a three-phase CHB-NPC multilevel inverter is considered. Single-phase model of this inverter is proposed in [8]. The individual DC-Links are produced by PV modules in this paper. Block diagram of the utilized inverter is shown in Fig.1. As it can be seen in this figure, each phase consists of two H-bridges that are connected in series and feeding by two PV modules. HB cells are constructed by two parallel 3-level NPC, which can generate five voltage level at the output. Switching command of each 3-level NPC, x_{mn} and y_{mn}, is [-1, 0, 1]. Where n and m determine the cell number and its phase respectively while, x and y specify the 3-level NPCs of each HB. The output voltage levels of HBs are including $[-1,-0.5,0,0.5,1]\times V_{m.n}^{dc}$ and it can be expressed as follow:

$$V_{m.n}^{cell} = \frac{1}{2}(x_{mn} - y_{mn}) \times V_{m.n}^{dc} \tag{1}$$

As it can be realized, each H-bridge cell has nine possible switching combination. Therefore, each phase has 9^N possible switching combination, where N is the number of H-bridge cells in each phase and it has two in this paper. Hence, total switching combination of the inverter is 9^{3N}. Each phase of the inverter can produce nine voltage level at the output that is summation of cell voltages. CHB-NPC is connected through an inductor and its resistor to the grid lines, hence

$$V_{m.g}^{inv} = V_{m.g}^{grid} + Ri_m + L\frac{di_m}{dt} \tag{2}$$

$$V_{m.o}^{inv} = \sum_{n=1}^{N} \frac{1}{2}(x_{m.n} - y_{m.n}) \times V_{m.n}^{dc} \tag{3}$$

$V_{m.g}^{inv}$ and $V_{m.o}^{inv}$ indicate the output voltage of inverter respect to the grid ground (g) and inverter neutral point (O) respectively. i_m is the line current of phase m, where m is "a", "b" or "c". L and R are the inductance of inductor and its resistance that connect the inverter phases to the grid lines. $V_{o.g}$ is called as common-mode voltage and it is defined as

$$V_{o.g} = \frac{1}{3}\sum_{m=[a,b,c]}(V_{inv,mO}) \tag{4}$$

By using Clarke transformation, the plant model can be expressed by vector equation

$$\begin{bmatrix}\alpha\\ \beta\end{bmatrix} = \frac{2}{3}\begin{bmatrix}1 & -1/2 & -1/2\\ 0 & \sqrt{3}/2 & -\sqrt{3}/2\end{bmatrix}\begin{bmatrix}a\\ b\\ c\end{bmatrix} \tag{5}$$

Therefore, equation (2) can be rewritten as follows

$$V_{m.g.[\alpha,\beta]}^{inv} = V_{m.g.[\alpha,\beta]}^{grid} + Ri_{m[\alpha,\beta]} + L\frac{di_{m[\alpha,\beta]}}{dt} \tag{6}$$

B. Reference Obtaining Procedure

As it mentioned before, PV modules are used to produce individual DC-Links. Therefore, obtaining the maximum available power and increasing the efficiency of PV modules are important issues to be considered. Among many control methods, perturb and observe (P&O) technique is a well-known and relatively effective one [20]. In this paper, an improved P&O method, which is proposed by [20], is used to control PV modules and obtain their voltage references. Respect to the conventional P&O, this method will enhance the controller response to atmospheric condition changes. Flowchart of the employed method is presented in Fig.2.

In order to transfer the harvested power from PV modules to the grid side, AC current reference should be generated. Both power flows, the harvested from PVs and injected to the grid, will affect DC-link voltage of HB modules. In this regard, the references of the injected currents to the grid can be obtained by observing DC-link capacitor voltages. The utilized method to generate current reference is presented in Fig.3, which is a PI based control method. This method guarantees the power balancing between PVs and the grid moreover it prevents capacitors from being discharged or overcharged.

To minimize the imbalances between the achievable powers in different phases, two areas are considered for PV arrays. PV arrays in the same vicinity have the closet radiation and temperature. However, to prevent imbalance current injection to the grid lines, if any mismatch happens between

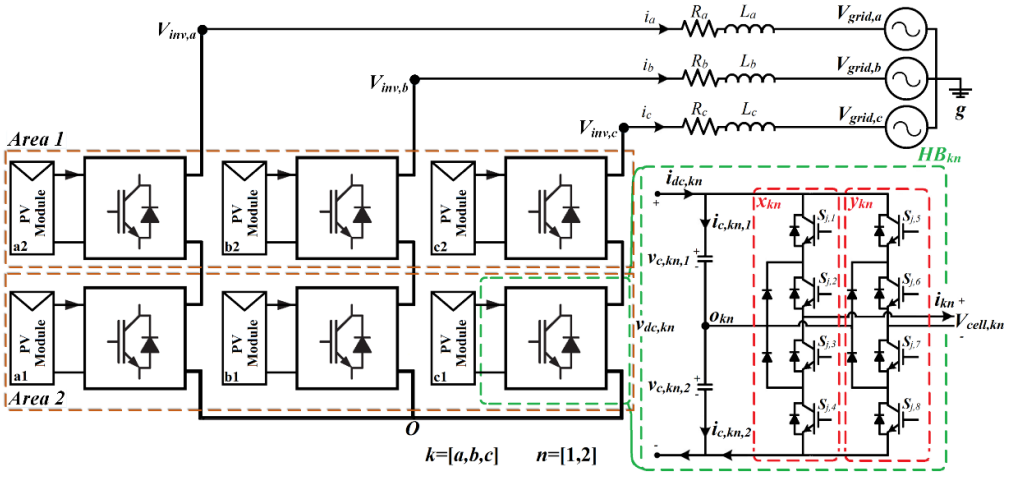

Fig. 1. Black diagram of PV-modules and grid tied three-phase 9-level CHB-NPC

phases, minimum obtained current reference should be applied to the output.

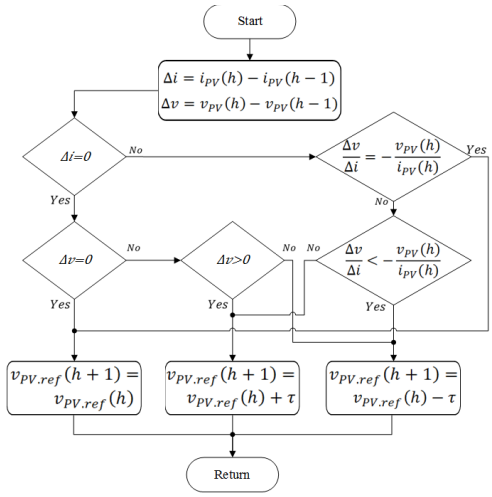

Fig. 2 Voltage reference obtaining of PV arrays using improved P&O procedure

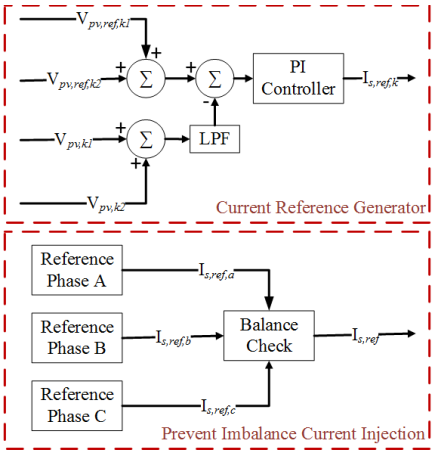

Fig. 3. PI based current reference generator

III. FCS-MPC

In the CHB converter, it is necessary to control the derived power from each module. In this paper, this matter can be handled by regulating the DC voltage of PV modules. In this regard, DC-link voltage regulation and output current tracking are the major tasks to be considered in the controller and its cost function. Besides the DC-Link voltages, capacitor voltages in each three-level NPC have to be balanced. In the conventional predictive control method, one cost-function is defined for each control objective and, the total cost function is a summation of individual cost functions with different weighting factors. Related cost function (CF) for each task can be defined as follow:

$$CF_{i_s} = (i_{s,ref,\alpha} - i_{s,\alpha}^{k+1})^2 + (i_{s,ref,\beta} - i_{s,\beta}^{k+1})^2 \quad (7)$$

$$CF_{v_{pv,m.n}} = (v_{pv,ref,mn} - (v_{c,mn,1}^{k+1} + v_{c,mn,2}^{k+1}))^2 \quad (8)$$

$$CF_{v_{o,m.n}} = (v_{c,mn,1}^{k+1} - v_{c,mn,2}^{k+1})^2 \quad (9)$$

In the above equations, CF_{i_s} is the cost-function of injected current to the grid and, to obtain the MPPT operation, DC-Link voltages of PV modules are regulated via $CF_{v_{pv,mn}}$. $CF_{v_{o,m.n}}$ checks the capacitor voltage balancing for HB modules, where $(k+1)$ indicates the future value of the control parameters.

The discrete model of equation (6) has been written as equation (10) and the prediction of currents can be estimated as equations (11) and (12).

$$V_{[\alpha,\beta]}^{inv(k)} = V_{[\alpha,\beta]}^{grid(k)} + Ri_{[\alpha,\beta]}^{k} + L\frac{i_{[\alpha,\beta]}^{k+1} - i_{[\alpha,\beta]}^{k}}{\Delta t} \quad (10)$$

Where, Δt is the sampling time (T_s) and k refers to the present value of the parameters.

$$i_{\alpha}^{(k+1)} = \frac{T_s}{L}\left(V_{\alpha}^{inv(k)} - V_{\alpha}^{grid(k)} - Ri_{\alpha}^{k}\right) + i_{\alpha}^{k} \quad (11)$$

$$i_{\beta}^{k+1} = \frac{T_s}{L}\left(V_{\beta}^{inv(k)} - V_{\beta}^{grid(k)} - Ri_{\beta}^{(k)}\right) + i_{\beta}^{(k)} \quad (12)$$

Three tasks should be considered to control the capacitor voltages, PV current, phase current and, switching state of each module. Due to the relation between capacitor voltage and its current, $c\frac{dv_c}{dt} = i_c$, module voltage variations can be calculated respect to the PV array current and phase current of the inverter. These currents are assumed to be constant in each control cycle. PV current always flows in to the two series capacitors of the HB modules and, phase current will affect the DC-link voltages respect to the voltage level of HB module. As previously mentioned, HB module voltage level can be defined as a function of its 3-level NPC commands. Prediction of DC-link voltages can be estimated as follow:

$$V_{mn}^{dc(k+1)} = V_{mn}^{dc(k)} + \frac{T_s}{C}(2i_{mn}^{pv(k)} - (x_{mn} - y_{mn})i_m^{(k)}) \quad (13)$$

The PV current would not affect the capacitor voltage balancing, since it is equally flowed in to both capacitors of DC-link. Hence, it can be said that the neutral point voltage in each HB module is varied just by phase current. However, phase current would not change the neutral point voltage if the voltage level of the HB module is zero or ±2. The future value of neutral point voltage can be calculated as follow:

$$V_{o.m.n}^{k+1} = \left(V_{c.m.n.2}^{(k)} - V_{c.m.n.1}^{(k)}\right) + \frac{T_s}{C}((x_{mn} + y_{mn})(x_{mn} - y_{mn})i_m) \quad (14)$$

The total cost function can be determined as follow:

$$CF_{total} = CF_{i_s} + \lambda_1 CF_{v_{pv,m.n}} + \lambda_2 CF_{v_{o,m.n}} \quad (15)$$

Where λ is the weighting factor.

In the conventional FCS-MPC, the cost function will be investigated for all switching states to find the optimal solution. As can be considered, with increasing the number of states, the calculation burden of the FCS-MPC will increase. This drawback will affect the overall performance of the controller. Besides high computation burden, tuning the weighting factors is another obstacle which should be taken into account. These weighting factors indicate the importance of each term in the cost function and control the variation of each control parameter respect to the other ones.

The reduction of the computational burden in the proposed method is discussed in the following section. As

latterly can be considered, weighting factors are eliminated in the proposed method.

IV. Proposed Method

The utilized inverter in this paper has 81 switching states per phase and 81^3 states in total. Searching these large number of states to find the optimal result in an adequate time seems to be impossible. As execution time of the control cycle increases, the capability of the controller degrades. In this regard, minimization of the execution time will enhance the controller operation. In order to address this problem, the proposed strategy divides the control procedure to three stages. First stage will be dealt with the output current of the inverter and, the second and third stages will be regulated DC-links voltages and balanced the capacitors voltages respectively.

A. First stage: output current and voltage

Due to the equations (11) and (12), the output voltage of the converter is the main parameter that affect the injected current to the grid. Equations (13) and (14) reveal that the output voltage of the converter has no effect on the DC voltage regulation or capacitor voltage balancing. In this regard, the output current and voltage vector are the first control objective and control parameter to be taken into account.

If we assume the same voltage in DC-links, each phase of the inverter has 9 voltage level. The combination of different phase voltage levels and using Clarke transformation clarifies that the inverter has 9^3 or 729 voltage vectors at its output. Investigation of the obtained vectors shows; there are only 217 individual voltage vectors from the total number of voltage vectors, 216 active voltage vectors (none zero vectors) and one zero voltage (Fig.4). As a result, only checking the individual voltage vectors will be enough for controlling the output current of the inverter, and hence the number of searched voltage vectors in each control cycle will be decreased. To reduce the number of searched voltage vectors a limited area around the last optimal point (the last optimal voltage vector) has been considered. In this paper, only six nearest voltage vectors to the optimal voltage vector in the last control cycle are considered (as shown in Fig.4). In this way, in each control cycle only seven voltage vectors out of 729 voltage vectors are investigated to control the output current, one central and 6 nearest voltage vectors. At last, the voltage vector that minimize the cost function of equation (7) will be selected. The nearest voltage vectors to each point can be detected either online or by a lookup table (the second approach is more suitable). In addition to fewer number of searched states, the voltage regulation equations are not attended in this stage and, the current equations has been eliminated in the other stages, which eventuate to reduction of execution time even more. Two more stages are discussed in the following parts to control the PV voltages and to balance the capacitors voltages.

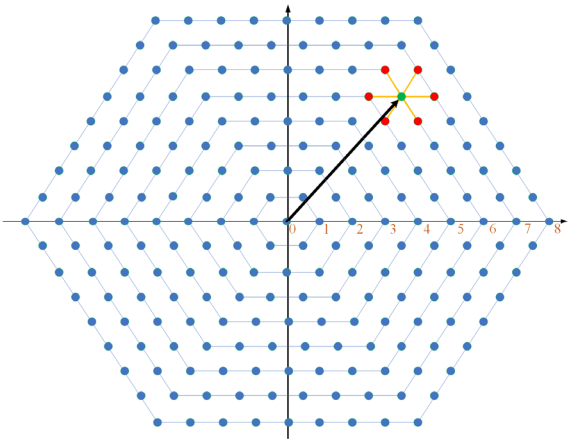

Fig.4. Voltage vectors of the 3-phase 9-level CHB-NPC

B. Redundancy selection

As mentioned above, each possible voltage vector has a number of redundancies. Considering Fig.4, eight hexagons can be observed in the space vector. Assume another hexagon at zero voltage, these hexagons can be numbered from the zero for the inner hexagon to the 8 for the outer one (Z=[0,1,…,8]). The voltage vectors in each hexagon have 9-Z redundancies. In other words, there are 9-Z different voltage levels in phases that will produce the same voltage vector in the output. Redundancies of each voltage vector can be identified respect to the voltage levels in three phases. For further explanation, phase voltage levels of $[l_{a,1},l_{b,1},l_{c,1}]$ and $[l_{a,2},l_{b,2},l_{c,2}]$ generate the voltage vectors at the output if $[l_{a,1}-l_{b,1},l_{b,1}-l_{c,1}]=[l_{a,2}-l_{b,2},l_{b,2}-l_{c,2}]$,where l_m is the phase voltage level of phase m. e.g. [-4,2,3] and [-3,3,4]. Beside vector redundancies, voltage level of each phase has its own redundant states, which are different combination of HB modules (As shown in Table I). As it can be considered in equation (13), HB module's voltage level affects its DC-Link voltage. In this regard, the DC-link voltages has to be controlled by selecting the appropriate phase voltage levels which leads to previously chosen voltage vector. As it can be realized, the suitable voltage vector redundancy and voltage level combination of the HB modules for each phase are selected in this stage to regulate the DC-link voltages. Combination of voltage vector redundancies and different voltage level of HB modules may lead to a large number of states and impose high computational burden to the controller. In order to prevent nested loops in control cycle and achieve a more targeted search algorithm, two stages are considered to select the voltage vector redundancy and voltage level of each HB module. In the second stage, to find the appropriate redundancy of the previously chosen voltage vector among its redundancies, the effect of different states on the summation of DC-links voltage are taken into account. Hence, cost function in equation (16) is defined. In this way, optimal voltage level of the phases that produce the desired voltage vector is selected. In the worst case, where zero

Table I. Voltage level of each HB respect to phase voltage level

Phase voltage level	[HB1,HB2]	[HB1,HB2]	[HB1,HB2]	[HB1,HB2]	[HB1,HB2]
0	[0, 0]	[-1, +1]	[+1, -1]	[-2, +2]	[+2, -2]
±1	[±1, 0]	[0, ±1]	[±2, ∓1]	[∓1, ±2]	---
±2	[±1, ±1]	[±2, 0]	[0, ±2]	---	---
±3	[±1, ±2]	[±2, ±1]	---	---	---
±4	[±2, ±2]	---	---	---	---

voltage is intended, cost function in equation (16) will be checked for nine possible states. However, at nominal operation, when voltage vector is expected to be between hexagons 6 to 8, the number of investigated states will be less than three.

$$CF_{v_l}=\left(\frac{T_s}{C}\left(-l_m^{(k+1)}i_m+2\sum_{n=1,2}i_{m.n}^{pv(k)}\right)+\sum_{n=1,2}v_{m.n}^{pv(k)}-\sum_{n=1,2}v_{m.n}^{ref.pv}\right)^2 \quad (16)$$

Where l_m is the voltage level of the three phases.

At the third stage, different combinations of HB modules are investigated to produce the desired voltage levels in each phase which are chosen in second stage. When zero voltage level is needed, maximum number of states will be occurred (five states). Since there is 120° phase difference between voltages angles, total number of search states for three phases are expected to be less than ten times. The following cost function is used to find the optimal combination of HB modules.

$$CF_{v_{HB}}=\left(\frac{T_s}{C}\left(2i_{m.n}^{pv}-l_{m.n}^{HB(k+1)}i_m\right)+v_{m.n}^{pv}-v_{m.n}^{ref.pv}\right)^2 \quad (17)$$

Where $l_{m.n}^{HB}$ is the voltage level of HB modules presented in Table I. The proposed cost function in equation (17) is individually investigated for different phases and optimal combination for the required voltage level will be selected. As mentioned above, equation (17) is expected to be checked less than 10 times.

In this way for each step only a few number of states are investigated. Furthermore, the proposed procedure eliminates the weighting factors selection.

V. Simulations and Results

In order to validate the effectiveness of the proposed control procedure, simulations are carried out in MATLAB-Simulink environment. The proposed method compared with the conventional one in steady state and transient conditions. System characteristics of the utilized systems are summarized in Table II. Although the proposed method has a much lower execution time but the same sampling frequency of 5_{KHz} is considered for both conventional and the proposed methods.

Table II: System parameters

Grid line parameters	*value*	*Inverter & PV parameters*	*value*
Line inductor, L	*2.5 mH*	*DC-link capacitors, C*	*3.3 mF*
Line resistor, R	*0.08 Ω*	*PV open-circuit voltage, V_{oc}*	*43.9 V*
Grid frequency, f_s	*50 Hz*	*PV short-circuit current, I_{sc}*	*5.3 A*
Phase voltage, V_s	*220 V*	*nom. MPPT Voltage, V_N*	*36.2V*
Phase current, I_s	*60 A*	*nom. MPPT Current, I_N*	*4.85 A*

A. Steady state condition

The radiation and temperature of PV arrays in the nominal condition is $1000\,W/m^2$ and $25^{\circ}C$ respectively. Results of different control methods are presented in Fig.5 to Fig.6. Steady state voltage of DC-links in MPPT operation is 217_v and maximum achievable power from each array is about 4200 watts. Fig.5.b and Fig.6.b show the DC-links voltages in phase A. As can be seen, the proposed and the conventional methods track the maximum power point of PV arrays and present the 217_v in DC-Links terminal. Additionally, the peak to peak voltage ripple for the conventional and the proposed methods are 16.4 and 16 volts respectively. Therefore, conventional method with searching all states and the proposed targeted control procedure achieve the same voltage ripple in the capacitors which is about 3.75%. The RMS of output current is about 56.5_A for all cases while THD of the conventional and proposed methods are 1.6% and 1.65%

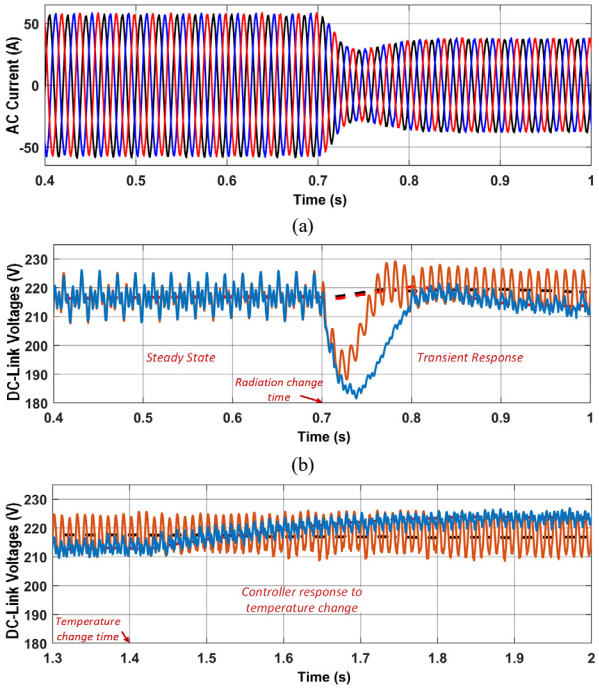

Fig.5. The conventional method results, a) injected AC current to the gird, b) DC link voltage in stady state and controller response to radation change, c) controller respose to the tempreature change.

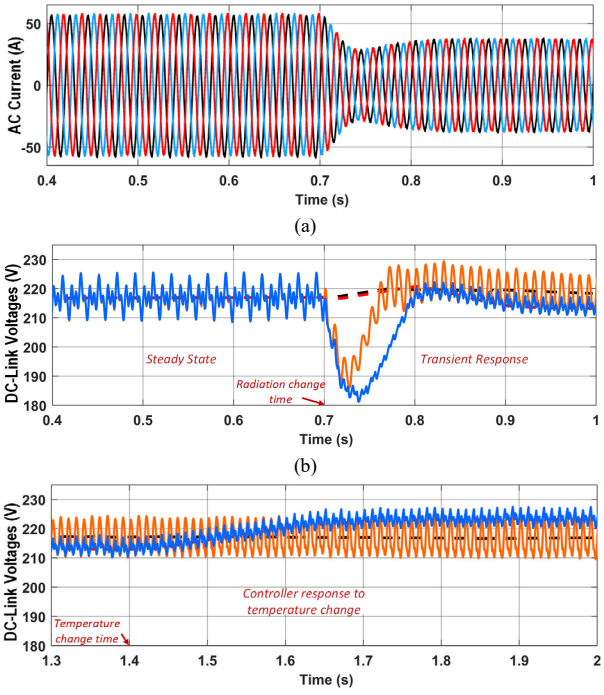

Fig.6. The proposed method results, a) injected AC current to the gird, b) DC link voltage in stady state and controller response to radation change, c) controller respose to the tempreature change.

respectively. The achieved results reveal the performance of the proposed method in the steady state condition.

B. Transient condition

Two different changes are applied for transient condition. At first, in 0.7s, radiation of the second area is decreased from 1000 to $300W/m^2$ and, secondly its temperature is decreased by $10^{\circ}C$ at 1.4s. In the first transient condition the voltage of PV arrays in area.2 should decrease to 213.5_{v} and area.1 should not change. Fig.5.b and Fig.6.b show the operation of both control methods which is achieved the desired voltages in PV arrays. DC-link voltage ripple in the area.1 is the same as previous and it is about 3.7% however DC-link voltage ripple in the area.2 for the conventional method is 2.2% while, for the proposed methods it is a little bit lower than that and is about 2%. The RMS of output current is 36.8A and its THD for the conventional method is 1.85% and for the proposed method it is 1.9%. After reduction of temperature in area.2, voltages of PV arrays should increase and, as it presented in Fig.5.c and Fig.6.c, the proposed method tracks the MPP of PV arrays and inject the desired current to the grid lines.

As can be considered, the proposed targeted method attains the same control performance with much lower computation effort. It is noteworthy that the lower computation burden leads to a higher sampling frequency. This improvement will enhance the controller's performance in practice.

VI. Conclusion

This paper aims to improve the overall performance of the finite set control model predictive control method. Therefore, the two main obstacles of this control method are taken into account. At first, high computational burden reduction considered and weighting factors are eliminated along with it. The lower execution time leads to higher sampling frequency that is an essential issue in FCS-MPC performance. Hence, the targeted proposed search method divides the conventional procedure into three steps. Each step deals with one control objective also, much lower calculations executed to fulfill each step. The proposed method explained for a grid-tied nine-level converter in which its DC-links are fed from PV modules. In the end, MATLAB-Simulink simulation results compared with the conventional method that illustrates the performance of the proposed method.

References

[1] Abu-Rub, Haitham, Joachim Holtz, Jose Rodriguez, and Ge Baoming. "Medium-voltage multilevel converters—State of the art, challenges, and requirements in industrial applications." *IEEE Transactions on Industrial Electronics* 57, no. 8 (2010): 2581-2596.

[2] Perez, Marcelo A., Steffen Bernet, Jose Rodriguez, Samir Kouro, and Ricardo Lizana. "Circuit topologies, modeling, control schemes, and applications of modular multilevel converters." *IEEE transactions on power electronics* 30, no. 1 (2014): 4-17.

[3] Alexander, Albert, and Manigandan Thathan. "Modelling and analysis of modular multilevel converter for solar photovoltaic applications to improve power quality." *IET renewable power Generation* 9, no. 1 (2014): 78-88.

[4] Islam, Md Rabiul, A. M. Mahfuz-Ur-Rahman, Kashem M. Muttaqi, and Danny Sutanto. "State-of-the-Art of the Medium-Voltage Power Converter Technologies for Grid Integration of Solar Photovoltaic Power Plants." *IEEE Transactions on Energy Conversion* 34, no. 1 (2018): 372-384.

[5] Rong, Fei, Xichang Gong, and Shoudao Huang. "A novel grid-connected PV system based on MMC to get the maximum power under partial shading conditions." *IEEE Transactions on Power Electronics* 32, no. 6 (2016): 4320-4333.

[6] Xiao, Bailu, Lijun Hang, Jun Mei, Cameron Riley, Leon M. Tolbert, and Burak Ozpineci. "Modular cascaded H-bridge multilevel PV inverter with distributed MPPT for grid-connected applications." *IEEE Transactions on Industry Applications* 51, no. 2 (2014): 1722-1731.

[7] Siwakoti, Yam P., Fang Zheng Peng, Frede Blaabjerg, Poh Chiang Loh, Graham E. Town, and Shuitao Yang. "Impedance-source networks for electric power conversion part II: Review of control and modulation techniques." *IEEE Transactions on Power Electronics* 30, no. 4 (2014): 1887-1906.

[8] Kakosimos, Panagiotis, Konstantinos Pavlou, Antonios Kladas, and Stefanos Manias. "A single-phase nine-level inverter for renewable energy systems employing model predictive control." *Energy conversion and management* 89 (2015): 427-437.

[9] Sultana, W. Razia, Sarat Kumar Sahoo, Sukruedee Sukchai, S. Yamuna, and D. Venkatesh. "A review on state of art development of model predictive control for renewable energy applications." *Renewable and sustainable energy reviews* 76 (2017): 391-406.

[10] Rodriguez, Jose, Marian P. Kazmierkowski, Jose R. Espinoza, Pericle Zanchetta, Haitham Abu-Rub, Hector A. Young, and Christian A. Rojas. "State of the art of finite control set model predictive control in power electronics." *IEEE Transactions on Industrial Informatics* 9, no. 2 (2012): 1003-1016.

[11] Preindl, Matthias, Erik Schaltz, and Paul Thogersen. "Switching frequency reduction using model predictive direct current control for high-power voltage source inverters." *IEEE Transactions on Industrial Electronics* 58, no. 7 (2010): 2826-2835.

[12] Vazquez, Sergio, Jose Rodriguez, Marco Rivera, Leopoldo G. Franquelo, and Margarita Norambuena. "Model predictive control for power converters and drives: Advances and trends." *IEEE Transactions on Industrial Electronics* 64, no. 2 (2016): 935-947.

[13] Rashwan, Ahmed, Mahmoud A. Sayed, Youssef A. Mobarak, Gaber Shabib, and Tomonobu Senjyu. "Predictive controller based on switching state grouping for a modular multilevel converter with reduced computational time." *IEEE Transactions on Power Delivery* 32, no. 5 (2016): 2189-2198.

[14] Veysinejad, Aria, Saman Rahmati, and Sadegh Shamlou. "Predictive Direct Torque Control with Reduced Number of Considered States in Synchronous Reluctance Motor Drive." In *2019 10th International Power Electronics, Drive Systems and Technologies Conference (PEDSTC)*, pp. 90-95. IEEE, 2019.

[15] Veysinejad, Aria, Saman Rahmati, and Mohammad Tavakoli Bina. "Predictive Direct Torque Control with Reduced Number of Predictions for a Three-level Inverter Driven Permanent Magnet Synchronous Motor." In *2019 27th Iranian Conference on Electrical Engineering (ICEE)*, pp. 813-818. IEEE, 2019.

[16] Böcker, Jan, Benjamin Freudenberg, Andrew The, and Sibylle Dieckerhoff. "Experimental comparison of model predictive control and cascaded control of the modular multilevel converter." *IEEE Transactions on Power Electronics* 30, no. 1 (2014): 422-430.

[17] Osman, Ilham, D. Xiao, M. F. Rahman, and Md Habibullah. "A two-stage optimal vector selection method for predictive torque control of a three-level VSI driven induction motor." In *2017 Australasian Universities Power Engineering Conference (AUPEC)*, pp. 1-6. IEEE, 2017.

[18] Gutierrez, Bryan, and Sang-Shin Kwak. "Modular multilevel converters (MMCs) controlled by model predictive control with reduced calculation burden." *IEEE Transactions on Power Electronics* 33, no. 11 (2018): 9176-9187.

[19] Cortes, Patricio, Alan Wilson, Samir Kouro, Jose Rodriguez, and Haitham Abu-Rub. "Model predictive control of multilevel cascaded H-bridge inverters." *IEEE Transactions on Industrial Electronics* 57, no. 8 (2010): 2691-2699.

[20] Shadmand, Mohammad B., Robert S. Balog, and Haitham Abu-Rub. "Model predictive control of PV sources in a smart DC distribution system: Maximum power point tracking and droop control." *IEEE Transactions on Energy Conversion* 29, no. 4 (2014): 913-921.